Journal of Geochemical Exploration 159 (2015) 48–61

Contents lists available at ScienceDirect

Journal of Geochemical Exploration

journal homepage: www.elsevier.com/locate/jgeoexp

Gahnite composition as a means to fingerprint metamorphosed massive sulfide and non-sulfide zinc deposits

Joshua J. O'Brien [a], Paul G. Spry [a,*], Graham S. Teale [b], Simon E. Jackson [c], Alan E. Koenig [d]

[a] Department of Geological and Atmospheric Sciences, 253 Science I, Iowa State University, Ames, IA 50011-3212, USA
[b] Teale & Associates, P.O. Box 740, North Adelaide, SA 5006, Australia
[c] Natural Resources Canada, Geological Survey of Canada, 601 Booth Street, Ottawa, ON K1A 0E8, Canada
[d] U.S. Geological Survey, Denver Federal Center, Denver, CO 80225, USA

ARTICLE INFO

Article history:
Received 11 April 2015
Revised 30 July 2015
Accepted 21 August 2015
Available online 28 August 2015

Keywords:
Gahnite
Trace elements
Metamorphosed sulfides
Exploration

ABSTRACT

Gahnite occurs in and around metamorphosed massive sulfide (e.g., Broken Hill-type Pb–Zn–Ag (BHT), volcanogenic massive sulfide Cu–Zn–Pb–Au–Ag (VMS), sedimentary exhalative Pb–Zn (SEDEX)), and non-sulfide zinc (NSZ) deposits. In addition to occurring in situ, gahnite occurs as a resistate indicator mineral in unconsolidated sediments (e.g., glacial till) surrounding such deposits. The spatial association between gahnite and metamorphosed ore deposits has resulted in its use as an empirical exploration guide to ore. Major and trace element compositions of gahnite from BHT, NSZ, SEDEX, and VMS deposits are used here to develop geochemical fingerprints for each deposit type.

A classification tree diagram, using a combination of six discrimination plots, is presented here to identify the provenance of detrital gahnite in greenfield and brownfield terranes, which can be used as an exploration guide to metamorphosed massive sulfide and non-sulfide zinc deposits. The composition of gahnite in BHT deposits is discriminated from gahnite in SEDEX and VMS deposits on the basis of plots of Mg versus V, and Co versus V. Gahnite in SEDEX deposits can be distinguished from that in VMS deposits using plots of Co versus V, Mn versus Ti, and Co versus Ti. In the Sterling Hill NSZ deposit, gahnite contains higher concentrations of Fe^{3+} and Cd, and lower amounts of Al, Mg, and Co than gahnite in BHT, SEDEX, and VMS deposits. Plots of Co versus Cd, and Al versus Mg distinguish gahnite in the Sterling Hill NSZ deposit from the other types of deposits.

1. Introduction

Geochemical fingerprints of resistate indicator minerals allow explorationists to search for various types of commodities covered by recently deposited unconsolidated sediments (e.g., alluvium, colluvium, and glacial till). For example, detrital grains of gahnite have been used in the search for metamorphosed massive sulfide deposits concealed beneath glacial till (e.g., Hicken et al., 2013a,b; McClenaghan, 2005; McClenaghan et al., 2012; Morris et al., 1997). The dispersal of indicator mineral suites from various ore types is well documented for porphyry copper deposits (e.g., apatite, magnetite, rutile, tourmaline, zircon), Ni–Cu–PGE deposits (e.g., chromite, diopside, Cr-rich enstatite, forsterite), diamond-bearing kimberlites (e.g., chromite, entstatite, forsterite, garnets, Mg-ilmenite, omphacite), and metamorphosed massive sulfide deposits (e.g., gahnite, willemite, franklinite, zincian staurolite) (Averill, 2001, 2007, 2011; McClenaghan and Kjarsgaard, 2001). However, despite the use of these indicator minerals as empirical guides to mineralization, such minerals are also found in rocks unrelated to mineralization. This has led to the use of major and trace element compositions of minerals to further refine their use as guides in exploration or in determining their provenance.

In particular, discrimination plots using major and trace element compositions have been used to infer the provenance of, for example, garnet (e.g., Aubrecht et al., 2009; Krippner et al., 2014), rutile (e.g., Scott and Radford, 2007), Cr-spinel (e.g., Aubrecht et al., 2009), magnetite (e.g., Dupuis and Beaudoin, 2011), and Zn-spinel (e.g., Heimann et al., 2005; Spry and Scott, 1986). In the case of garnet, the composition of the so-called "G-10" garnets, which are distinguished from other garnet compositions on the basis of a plot of wt.% Cr_2O_3 versus CaO, has been instrumental in exploring for diamonds (e.g., Gurney, 1984). Furthermore, using the trace element composition of magnetite, Dupuis and Beaudoin (2011) developed a series of discrimination diagrams to identify compositional differences for magnetite from various types of ore deposits.

Although the presence of gahnite (AB_2O_4), where A = Zn^{2+}, Fe^{2+}, Mg^{2+}, and lesser amounts of Mn^{2+}, where Zn > (Fe + Mg + Mn), and B = Al^{3+} and to a lesser extent Fe^{3+}, has long been used as an empirical exploration guide to ore (e.g., Sheridan and Raymond, 1984), it also occurs in a variety of sulfide-free rock types. Spry and Scott (1986), Heimann et al. (2005), and Spry and Teale (2009) used a ternary diagram, with Zn, Fe, and Mg as components, to identify

* Corresponding author.
E-mail address: pgspry@iastate.edu (P.G. Spry).

http://dx.doi.org/10.1016/j.gexplo.2015.08.005
0375-6742/

compositional ranges for gahnite in: (1) marble, (2) granitic pegmatites, (3) metabauxites, (4) unaltered and hydrothermally altered Fe–Al-rich metasedimentary and metavolcanic rocks, (5) Al-rich granulites, and (6) metamorphosed massive sulfide deposits. Despite being able to distinguish gahnite compositions associated with sulfide-bearing deposits from those in other rock types, the use of major element composition of gahnite alone has its limitations as an exploration guide because the composition of gahnite in sulfide-rich rocks is indistinguishable from the composition of gahnite in sulfide-poor rocks (O'Brien et al., 2015a,b).

In addition to gahnite occurring in situ in a variety of host rocks, it also occurs in unconsolidated sediments, including beach sands (e.g., Kaye and Mrose, 1965), glacial till (e.g., Morris et al., 1997), soil (e.g., Nachtegaal et al., 2005), and stream sediments (e.g., Crabtree, 2003). Identification of gahnite in the heavy mineral fraction separates of glacial till is facilitated by its green–blue color, high specific gravity (G = 4.55), hardness (8 on Moh's hardness scale), and chemical stability under oxidizing conditions (Hicken et al., 2013b; Morris et al., 1997). Morris et al. (1997) reported gahnite in glacial sediments in northwestern Ontario, where gahnite also occurs in situ in volcanogenic massive sulfide (VMS) (i.e., Mattabi and Geco) and sedimentary exhalative (SEDEX) (i.e., Hurdman Township) deposits, peraluminous granites, and granitic pegmatites. Using major element chemistry, Morris et al. (1997) attempted to determine the provenance of gahnite recovered from glacial sediments. However, gahnite compositions plot within the metamorphosed massive sulfide field of Spry and Scott (1986) in a Zn–Fe–Mg ternary diagram, and are unable to distinguish detrital gahnite derived from VMS deposits from those spatially associated with SEDEX deposits (Morris et al., 1997).

Recent studies by O'Brien et al. (2013, 2015a,b) utilized the trace element composition of gahnite (in conjunction with major elements), measured using laser ablation-inductively coupled plasma-mass spectrometry (LA-ICP-MS), as a potential exploration guide to Broken Hill-type (BHT) Pb–Zn–Ag deposits in the Broken Hill domain, Australia. They noted that variability in the trace element composition of gahnite was a function of different physicochemical conditions during gahnite growth, whole-rock geochemistry, pre-metamorphic alteration, and the chemistry of precursor minerals. Like other members of the spinel group (e.g., magnetite and chromite), the trace element chemistry of gahnite is dominated by the first series transition metals (i.e., Ti, V, Cr, Mn, Co, Ni), Ga, and Cd (Dupuis and Beaudoin, 2011; Nadoll et al., 2012; Nehring et al., 2010; Pagé and Barnes, 2009). No trace element compositions of gahnite from other metamorphosed massive sulfide deposits (e.g., SEDEX, VMS, and non-sulfide zinc (NSZ) deposits) have previously been obtained.

The primary objective of this study is to show how a series of compositional discrimination plots, presented as a tree diagram, can be used to distinguish the composition of gahnite among the following deposit types: BHT (i.e., Broken Hill, Australia; Broken Hill, South Africa; Melbourne Rockwell, Australia; and Mutooroo, Australia), VMS (i.e., Mamandur, India; Kvänberget, Sweden; several small Proterozoic Cu–Zn deposits, Colorado (i.e., Bon Ton, Caprock, Cotopaxi, Independence, and Sedalia)), SEDEX (i.e., Angas, Australia; Foster River, Saskatchewan), and NSZ (Sterling Hill, New Jersey) (Fig. 1). We also analyzed gahnite from the Bleikvassli Zn–Pb–(Cu) deposit, Norway, and the Stollberg Zn–Pb–Ag + magnetite deposits, Sweden. It is noted here that some researchers consider Bleikvassli to be a SEDEX deposit (Cook et al., 1998; Lockington et al., 2014; Skauli, 1992, 1993). However, studies by Larsen et al. (1997) and Bjerkgård (1999) suggest the prominent microcline gneiss stratigraphically below the deposit is an alkali syenite, and that Bleikvassli is of the VMS-type. The Stollberg deposits formed as sub-sea floor replacement deposits in volcanic rocks spatially associated with carbonate rocks, and appear to have affinities with VMS deposits (Jansson et al., 2013). The origin of BHT deposits is controversial and several different genetic models have been proposed (see Greenfield, 2003). It has been suggested in the past that they are, for example, metamorphosed SEDEX deposits (e.g., Gustafson and Williams, 1981), but we consider them to be a separate class of deposit based on the classification schemes of Walters (1998), Greenfield (2003), Leach et al. (2005), and Spry et al. (2009). Utilization of the tree diagram developed here can be applied to the composition of detrital gahnite to determine their provenance, or the type of ore deposit from which they were derived. These geochemical fingerprints and the tree diagram will aid in the search for metamorphosed massive sulfide deposits in greenfield and brownfield terranes.

2. Sampling and analytical methods

Samples of gahnite from the Broken Hill (Australia) and Melbourne Rockwell (O'Brien et al., 2015b; Spry, 1978; Spry et al., 2010), Mutooroo

Fig. 1. Global map showing the location of gahnite-bearing deposits examined in this study: 1. Foster River, Saskatchewan; 2. several small Proterozoic Cu–Zn deposits, Colorado (i.e., Bon Ton, Caprock, Cotopaxi, Independence, and Sedalia); 3. Sterling Hill, New Jersey; 4. Bleikvassli, Norway; 5. Stollberg, Sweden; 6. Kvänberget, Sweden; 7. Broken Hill, South Africa; 8. Mamandur, India; 9. Mutooroo, Australia; 10. Angas, Australia; 11. Broken Hill, Australia; 12. Melbourne Rockwell, Australia.

Table 1
Characteristics of gahnite-bearing metamorphosed base metal deposits.

Deposit	Deposit type[a]	Metamorphic facies	Deposit age	Tectonic setting	Host rock sequence	Sulfide assemblage[b]	References
Angas, Australia	SEDEX	Amphibolite	600–590 Ma?	Intracratonic basin/rift	Pelite, And–Grt–St ± Ghn–Schist, metagraywacke, banded iron formation, quartz–garnet rock	Po–Sp ± Gn ± Ccp	Both et al. (1995), Toteff (1999), Spry et al. (2010)
Foster River, Saskatchewan	SEDEX	Upper amphibolite	1.92–1.86 Ga	Back–arc basin	Psammite, pelite with quartzite, gahnite–rich rock, iron formation, quartz garnetite, and nodular sillimanite rock	Sp–Py–Po ± Gn ± Ccp	Coombe (1994), Steadman and Spry (2015)
Broken Hill, Australia	BHT	Granulite	1.695 Ga	Intracratonic rift	Pelite, psammite, felsic volcanoclastic rock, amphibolite	Gn–Sp–Ccp ± Asp ± Po	Johnson and Klingner (1975), Barnes et al. (1983), Haydon and McConachy (1987), Barnes (1988)
Broken Hill, South Africa	BHT	Amphibolite	1.64–1.2 Ga	Continental cratonic interior basin	Quartzitic, pelitic, psammitic metasedimentary rocks Amphibolites, leucocratic gneisses	Py–Po–Mrc–Sp–Gn–Ccp	Ryan et al. (1986), Spry (1987)
Melbourne Rockwell, Australia	BHT	Granulite	1.695 Ga	Intracratonic rift	Qz–Ghn lode horizon in Qz–Fsp–Bt ± Sil psammopelitic to pelitic metasedimentary rock	Cer ± Mag ± Mlc	Bartholomaeus (1987), Burton (1994)
Mutooroo, Australia	BHT	Granulite	1.696 ± 17 Ga	Intracratonic rift	Psammitic and pelitic schists, garnet–bearing quartzofeldspathic gneiss, blue quartz–gahnite rock	Po–Ccp ± Py ± Mag ± Ilm ± Sp	Spry et al. (2004)
Bleikvassli, Norway	VMS?	Upper amphibolite	1.00 Ga	Rifting margin of the Laurentian plate	Kyanite–garnet–mica schist, quartzofeldspathic gneiss, metaquartzite, amphibolite	Py–Po–Ccp–Sp–Gn ± Asp	Skauli (1992), Cook (1993), Rosenberg et al. (1998), Cook et al. (1998)
Colorado Cu–Zn Deposits, USA	VMS	Upper amphibolite	1.8–1.7 Ga	Island arc	Feldspar–rich gneiss (metafelsic volcanic rocks), amphibolite, sillimanite gneiss, calc–silicate gneiss	Sp–Ccp–Gn ± Py	Sheridan and Raymond (1984), Heimann et al. (2005)
Mamandur, India	VMS	Granulite	2.6 Ga		Pyroxene granulite, pelite, quartzofeldspathic gneiss	Sp–Ccp–Gn ± Po ± Ang	Chattopadhyay (1999), Simhachalam and Rao (2004), Ghosh et al. (2011)
Kvänberget, Sweden	VMS	Amphibolite	1.88–1.86 Ga	Continental margin or magmatic arc	Intermediate to felsic metavolcanic rocks overlying psammopelite	Ccp–Po–Sp	Hallberg et al. (2012)
Stollberg, Sweden	VMS?	Upper amphibolite	1.9 Ga	Extensional back arc basin	Bimodal felsic and mafic volcanic rocks overlying metasedimentary rocks	Sp–Gn ± Py ± Po ± Ccp ± Apy ± Mag	Allen et al. (1996), Jansson et al. (2013)
Sterling Hill, New Jersey	NSZ	Upper amphibolite to granulite	1.25–1.24 Ga	Back–arc basin	Franklin Marble (Wlm + Frk + Cal ± Znc); occurs near contact of underlying Cork Hill Gneiss	Wlm–Frk–Znc	Drake (1990), Johnson et al. (1990), Volkert et al. (2010)

Notes.
[a] Abbreviations for deposit type: BHT = Broken Hill–type; SEDEX = sedimentary exhalative; VMS = volcanogenic massive sulfide; NSZ = nonsulfide zinc.
[b] Mineral abbreviations after Whitney and Evans (2010); Ang = anglesite, Apy = arsenopyrite, Bt = biotite, Cal = calcite, Ccp = chalcopyrite, Cer = cerussite, Frk = franklinite, Fsp = feldspar, Ghn = gahnite, Gn = galena, Grt = garnet, Mag = magnetite, Mrc = marcasite, Mlc = malachite, Py = pyrite, Po = pyrrhotite, Qz = quartz, Sil = sillimanite, Sp = sphalerite, St = staurolite, Wlm = willemite, Znc = zincite.

(O'Brien et al., 2015b), Broken Hill (South Africa) (Spry, 1987), Bleikvassli (Rosenberg et al., 1998), central Colorado (Heimann et al., 2005), Foster River (Steadman and Spry, 2015), Angas (Spry et al., 2010), Kvänberget, Sterling Hill, and Stollberg are housed at Iowa State University. Samples from Kvänberget and Mamandur were collected from surface locations, whereas those from Sterling Hill were obtained from the open pit and mine dumps adjacent to the deposit. Gahnite from Stollberg was collected from drill core as part of an ongoing trace element study of silicates and oxides from massive sulfide deposits in the Stollberg district (Frank et al., 2014; O'Brien et al., 2014; Spry et al., 2015). Trace element concentrations of gahnite from Broken Hill (Australia), Mutooroo, and Melbourne Rockwell are in the electronic supplement of O'Brien et al. (2015b). The type, metamorphic facies, age, tectonic setting, host rock sequence and sulfide assemblage for each deposit are in Table 1, whereas the mineralogy of each sample is given in Table 2, except for those from Broken Hill (Australia), Mutooroo, and Melbourne Rockwell, which are given in O'Brien et al. (2015b).

Compositions of gahnite (MgO, Al_2O_3, SiO_2, TiO_2, MnO, FeO, ZnO) were measured using a JEOL JXA-8900 Electron Probe Microanalyzer (EPMA) at the University of Minnesota, operated with an accelerating voltage of 15 kV, a beam current of 20 nA, and a spot size of 1-2 μm, and using a range of mineral standards including gahnite (Zn, Al), pyrope (Si, Mg), hornblende (Ti), ilmenite (Fe), and spessartine (Mn). The beam time for background and peaks was 10 s each.

Concentrations of 52 elements were obtained for gahnite from BHT, SEDEX, and VMS deposits at the Geological Survey of Canada (Ottawa) using a LA-ICP-MS, comprising a Photon Machines "Analyte 193" excimer (Ar–F) laser ablation system coupled to an Agilent 7700 Series ICP-MS, fitted with a second rotary interface pump that approximately doubles instrument sensitivity. Compositions were obtained using a nominal spot size of 43, 52, 69, or 86 μm. Analyses were calibrated using an external standard, GSD-1G, a synthetic glass microbeam reference standard (USGS), whereas values of Al_2O_3 from EPMA analysis were used for internal standardization. GSD-1G was analyzed twice every 12–15 analyses of unknown samples to correct for instrument sensitivity drift. Analytical precision and accuracy were determined by analyzing reference material BCR-2G repeatedly throughout the day, under operating conditions identical to that used during routine gahnite analyses. Data reduction was performed using the computer program GLITTER (Van Achterbergh et al., 2001), which allows visual inspection and selective integration of time-resolved signal intensity profiles prior to conversion of integrated signals to concentrations using "GeoREM preferred values" for element contents of GSD-1G (http://georem.mpch-mainz.gwdg.de/).

Concentrations of the same 52 elements for gahnite from the Sterling Hill NSZ deposit were measured at the U.S. Geological Survey (Denver) using a LA-ICP-MS, comprising a New Wave Research UP-193 FX LA system (193-nm excimer) coupled to a PerkinElmer DRC-e ICP-MS. Data were obtained using a spot size of 85 and 150 μm, and calibrated

Table 2
Zincian spinel-bearing assemblages.

Deposit type		Deposit	Sample number	Assemblage
BHT				
	Broken Hill, S. Africa		PS84-003	Ghn–Qz–Ccp–Mag–Po–Sp
	Broken Hill, S. Africa		PS84-005	Qz–Ghn–Po–Mag–Sp–Gn–Py–Bt–Ms
	Broken Hill, S. Africa		PS84-006	Qz–Mag–Bt–Ghn–Sp–Gn–Po–Py
	Broken Hill, S. Africa		PS84-136	Qz–Grt–Ghn–Bt–Mag–Chl
	Broken Hill, S. Africa		PS84-151	Qz–Ghn–Po–Mag
	Broken Hill, S. Africa		PS84-153	Qz–Grt–Ghn–Po–Sp–Bt
	Broken Hill, S. Africa		PS84-154	Qz–Ghn–Po
NSZ				
	Sterling Hill		STER-10-01	Cpx–Ghn–Cal–Bt
	Sterling Hill		STER-10-02	Cal–Ghn–Cpx
	Sterling Hill		STER-10-04	Cpx–Cal–Ghn
	Sterling Hill		STER-10-05	Cpx–Ghn–Bt–Cal
SEDEX				
	Angas			
	Angas		ANG-098	Qz–Ghn–Grt
	Angas		ANG-099	Grt–Qz–Ghn–Bt
	Foster River			
		Sito East	FRSL-10131	Qz–Ghn–Py-retrograde Ms, Chl
		Sito East	FRSL-10188	Qz–Ghn–sulfides
		Sito East	FRSL-10191	Qz–Ghn–Sp–Py
		Sito East	FRSL-10247	Qz–Mc–Sil–Grt–Bt +/–Ghn–Po
		George	FRSL-10402	Qz–Fsp–Ghn
		George	JSGO-005	Qz–Ksp–Ghn–Sp-Bt
		Robyn Lake	JSRL-005	Qz–Grt–Bt–Ksp
		Sito West	JSSW-022	Qz–Grt–Bt–Ksp
VMS				
	Bleikvassli		JR95-004	Qz–Bt–Ms–Py–Ghn (Ap–Po–Sp–Gn–Ccp–Rt)
	Bleikvassli		JR95-008B	Bt–Chl–Grt–St–Po (Qz–Ap–Py–Sp–Gn–Ccp)
	Bleikvassli		JR95-012	Qz–Bt–Ghn–Ms–St–Po (Ap–Sp–Gn–Ccp–Rt)
			JR95-172	Ms–Pl–Po–Ghn (Qz–Bt–St–Sp–Ccp–Rt)
	Colorado			
		Cinderella	99CO-03	Ghn–Chl–Ath–Sil–Py
		Cinderella	99CO-05	Qz–Chl–Phl–Ghn–Kfs–Pl–Sil–(Grt)
		Bon Ton	99CO-23	Phl–Qz–Grt–Ghn–Pl–(Sil–Rt–Py–Ccp–Sp)
		Sedalia	99CO-38	Ged–Ghn–Chl–(Mag–Ilm–Py–Sp–Gn–Cv)
		Sedalia	99CO-39	Cum–Ghn–(Ilm–Ccp–Sp–Cv)
		Cotopaxi	99CO-72	Qz–Ghn–Sp–Gn–(Phl–Ccp–Po–Mo)
		Cotopaxi	99CO-76	Qz–(Phl–Bt–Sil–Ghn–Pl)
		Independence	AHCO-128	Ath–Phl–Ghn–(Rt–Ilm–Ccp–Po–Sp)
		Independence	AHCO-137	Ath–Phl–Ghn–(Sil–Chl–Zrn–Ilm–Mo)
		Caprock	AHCO-153	Phl–Grt–Ghn–(Rt–Ms)
	Kvänberget		70820	Qz–Ghn–Ged–Bt–(Cum–Po–Ccp–Mo–Zrn–Mnz)
	Mamandur		IP6551	Bt–Sp–Qz–Grt–Ghn–Pl–Py
	Mamandur		IP6553	Qz–Ghn–Grt–Bt–(sulfide)
	Mamandur		IP6563	Qz–Ghn–Pl–(Ccp–Bt–Gn)
	Stollberg		SSF21 408.5A	Bt–Ghn–Qz–Po–Sp
	Stollberg		SSF21 408.5B	Bt–Ghn–Qz–Po–Sp

Notes:
[1]Abbreviations for deposit type: BHT = Broken Hill-type; SEDEX = sedimentary exhalative; VMS = volcanogenic massive sulfide; NSZ = nonsulfide zinc.
[2]Mineral abbreviations after Whitney and Evans (2010); Ath = anthophyllite, Ap = apatite, Apy = arsenopyrite, Bt = biotite, Ccp = chalcopyrite, Chl = chlorite, Cpx = clinopyroxene, Cum = cummingtonite, Cv = covellite, Fsp = feldspar, Ged = gedrite, Ghn = gahnite, Gn = galena, Grt = garnet, Ilm = ilmenite, Ksp = K-feldspar, Mag = magnetite, Mc = microcline, Mlc = malachite, Mnz = monazite, Mo = molybdenite, Ms = muscovite, Phl = phlogopite, Pl = plagioclase, Po = pyrrhotite, Py = pyrite, Qz = quartz, Rt = rutile, Sil = sillimanite, Sp = sphalerite, St = staurolite, Znc = zincite, Zrn = zircon.
[3]Minerals listed in parentheses are present in trace amounts.

using external synthetic glass reference standards GSD-1G and NKT-1G from the U.S. Geological Survey. Values of Al_2O_3 from EPMA analysis were used for internal standardization. BCR-2G was analyzed as an unknown to test analytical precision and accuracy. The trace element composition of this standard is in Rocholl (2008). Concentrations were determined off-line using calculations outlined by Longerich et al. (1996). Detection limits for both LA-ICP-MS instruments are in Table 3. Those elements analyzed that were generally above detection limits were Cd, Co, Cr, Ga, Li, Mn, Ni, Pb, Ti, and V, whereas elements that were generally near or below detection limits were Ag, As, B, Ba, Be, Bi, Ge, Hf, Mo, Rb, S, Sb, Sc, Sn, Sr, W, Y, and Zr, as well as the rare earth elements.

3. Results

3.1. Major element chemistry

Representative major and minor element compositions of zincian spinels from various deposits are in Table 4. Using the same components as Spry and Scott (1986) and Heimann et al. (2005) (i.e., gahnite ($ZnAl_2O_4$), hercynite ($FeAl_2O_4$), and spinel sensu stricto ($MgAl_2O_4$)), relative proportions of Zn, Fe, and Mg for each analysis are presented here in a series of ternary plots, which are grouped on the basis of deposit type (Fig. 2). The data in these plots are overlain by the compositional fields of Heimann et al. (2005) for gahnite from various geological

Table 3
Average detection limits of LA-ICP-MS analyses and comparison between concentrations of trace elements in BCR-2G and those reported in the literature.

Element	Detection limits[1]				Detection limits[2]		BCR-2G[3]			
	43 μm	52 μm	69 μm	86 μm	85 μm	150 μm	Mean	Standard deviation	Literature values (ppm)*	Difference percentage
Li	2.67	1.65	1.35	0.76	1.03	0.36	9.1	0.538	9.00	1.40
Be	0.48	0.34	0.216	0.162	–	–	2.37	0.316	2.30	3.12
B	1.77	1.13	1.11	0.55	–	–	4.5	0.657	6.00	25.45
Na	–	–	–	–	6.0	2.40	–	–	–	–
Mg	1.58	1.09	0.75	0.53	0.96	0.288	21,600	305	20,980	2.96
Al	2.20	1.44	1.03	0.74	5.2	6.6	71,000	212	71,400	0.56
Si	58	49	22.9	18.1	1050	294	257,000	8412	253,000	1.58
S	<0.00000	<0.00000	<0.00000	<0.00000			<0.00000	<0.00000	–	–
P	–	–	–	–	42	9.8	–	–	–	–
K	2.78	1.62	1.55	0.87	69	17.9	14,800	372	14,900	0.67
Ca	–	–	–	–	137	45	–	–	–	–
Sc	0.138	0.083	0.060	0.042	0.60	0.276	35	0.947	33	6.06
Ti	0.59	0.39	0.242	0.182	2.588	1.071	13,300	230.138	14,100	5.67
V	0.072	0.046	0.0261	0.022	0.340	0.127	448	9.867	425	5.33
Cr	0.87	0.57	0.33	0.275	1.69	0.48	15.6	0.602	17.00	8.34
Mn	0.184	0.139	0.075	0.065	0.49	0.141	1570	30.309	1550	1.29
Fe	6.322	4.5	2.57	2.07	20.3	5.979	100,000	2007	96,600	3.52
Co	0.044	0.027	0.0156	0.0140	0.124	0.040	39	0.990	38	1.63
Ni	0.35	0.208	0.120	0.104	0.70	0.244	12.3	0.453	13.00	5.19
Cu	0.35	0.205	0.167	0.111	0.45	0.134	18.4	0.623	21.00	12.53
Zn	15.0	10.9	8.4	5.2	16.0	6.4	146	14.692	125	16.56
Ga	0.075	0.047	0.032	0.0247	0.284	0.084	22.5	0.699	23.00	2.23
Ge	0.62	0.38	0.270	0.194	0.44	0.129	1.82	0.168	1.50	21.49
As	0.287	0.199	0.151	0.084	0.89	0.208	0.77	0.102	–	–
Rb	0.0278	0.0178	0.0133	0.0088	0.112	0.0225	47	1.251	47	0.11
Sr	0.0074	0.0052	0.00258	0.00225	0.062	0.0162	342.599	6.845	342	0.18
Y	0.0083	0.0059	0.0030	0.00274	0.046	0.0200	34	0.944	35	1.71
Zr	–	–	–	–	0.089	0.042	–	–	–	–
Mo	0.0956	0.059	0.0288	0.0289	0.255	0.054	265	7.059	270	1.74
Ag	0.031	0.0196	0.0103	0.0099	0.192	0.064	0.76	0.149	0.50	51.29
Cd	0.122	0.092	0.050	0.040	2.631	0.437	0.148	0.036	0.50	70.32
Sn	0.057	0.041	0.0268	0.0191	0.191	0.066	1.74	0.083	2.60	33.06
Sb	0.030	0.0210	0.0096	0.0082	0.183	0.054	0.297	0.029	0.35	15.11
Ba	0.037	0.0277	0.0141	0.0121	0.142	0.048	660	14.926	683	3.37
La	0.0041	0.0032	0.00162	0.00144	0.0221	0.0081	25.2	0.468	24.70	1.96
Ce	0.0045	0.0033	0.00165	0.00138	0.0214	0.0064	53	1.131	53	0.43
Pr	0.0036	0.0027	0.00143	0.00130	0.0199	0.0063	6.61	0.125	6.70	1.41
Nd	0.0187	0.0137	0.0073	0.0061	0.096	0.042	28.7	0.625	28.90	0.56
Sm	0.0273	0.0182	0.0099	0.0086	0.120	0.045	6.61	0.168	6.30	4.97
Eu	0.0068	0.0055	0.00288	0.00243	0.0292	0.0112	1.96	0.051	1.91	2.71
Gd	0.0269	0.020	0.0093	0.0094	0.137	0.057	6.9	0.188	6.59	4.40
Tb	0.0035	0.00268	0.00124	0.00120	0.0256	0.0093	1.00	0.028	1.02	2.20
Dy	0.0154	0.0105	0.0054	0.0050	0.121	0.046	6.3	0.199	6.44	1.66
Ho	0.0036	0.0027	0.00141	0.00124	0.0188	0.0072	1.27	0.038	1.22	4.19
Er	0.0152	0.0117	0.0057	0.0057	0.068	0.0233	3.8	0.122	3.70	1.36
Tm	0.0031	0.0026	0.00132	0.00118	0.0177	0.006	0.50	0.015	0.51	1.89
Yb	0.0219	0.0173	0.0083	0.0082	0.124	0.054	3.4	0.105	3.20	5.86
Lu	0.0035	0.0025	0.00127	0.00121	0.0228	0.0084	0.50	0.017	0.50	1.28
W	0.0170	0.0121	0.0065	0.0059	0.087	0.031	0.53	0.029	0.50	6.94
Au	–	–	–	–	0.042	0.0115	–	–	–	–
Pb206	0.031	0.0283	0.0099	0.0094	–	–	10.8	0.448	11.00	1.92
Pb207	0.035	0.034	0.0120	0.0110	–	–	11.1	0.444	11.00	1.09
Pb208	0.0222	0.0198	0.0070	0.0060	0.055	0.0158	11.2	0.467	11.00	1.66
Bi	0.0074	0.0062	0.0034	0.00281	0.032	0.0070	0.051	0.006	0.05	1.00
Th	0.0049	0.0037	0.00189	0.00161	0.0232	0.0089	5.8	0.231	5.90	1.03
U	0.0046	0.0035	0.00182	0.00160	0.0209	0.0070	1.70	0.058	1.69	0.36

Notes:
[1]Detection limits of LA-ICP-MS at Geological Survey of Canada (Ottawa).
[2]Detection limits of LA-ICP-MS at USGS (Denver).
[3]BCR-2G values only from LA-ICP-MS at Geological Survey of Canada; BCR-2G values taken; from http://georem.mpch-mainz.gwdg.de/sample_query_pref.asp.

settings. Gahnite from BHT, SEDEX, and VMS deposits mostly plots within field 3 for gahnite in metamorphosed massive sulfide deposits hosted by hydrothermally altered Fe–Al-rich metasedimentary and metavolcanic rocks ($gahnite_{45–85}hercynite_{15–45}spinel_{0–20}$). Gahnite in VMS and SEDEX deposits generally contains a higher Mg content than gahnite from BHT deposits. However, some grains of gahnite from the Foster River, Broken Hill (Australia), and Colorado Cu–Zn deposits, contain a higher proportion of Fe, and plot within the field of unaltered and altered Fe–Al-rich metasedimentary and metavolcanic rocks (field 6). Moreover, some gahnite from central Colorado is Mg-rich and plots in the metamorphosed massive sulfide deposits and S-poor rocks in Mg–Ca–Al alteration zones field (field 2). The reason for this is that gahnite from this location occurs in Mg-rich alteration and the Mg spinel component is not buffered by fS_2–fO_2 conditions, which control the Zn:Fe ratio of zincian spinels (Spry and Scott, 1986). Similarly, those spinels that occur in or adjacent to a sulfide deposit that contain ~<1 wt.% Fe sulfides will be Fe-rich and fall within field 6. Gahnite from the Sterling Hill NSZ deposit contains low amounts of Al (50.2 wt.% Al_2O_3), Mg

Table 4
Representative major element compositions of gahnite from various deposit types[1].

Deposits[2]	BHT				SEDEX				VMS				NSZ
	1	2	3	4	5	6	7	8	9	10	11	12	13
n	n = 8	n = 2	n = 2	n = 7	n = 9	n = 4	n = 3	n = 6	n = 3	n = 5	n = 5	n = 1	n = 7
wt.% oxide													
Al_2O_3	56.46	55.62	55.72	55.92	55.77	55.62	56.32	56.67	60.88	57.41	54.66	57.85	50.22
FeO	11.81	8.21	7.77	7.45	7.52	6.22	21.66	6.89	6.07	10.03	17.99	9.73	6.83
MgO	1.64	1.05	0.67	1.32	2.31	1.79	3.83	2.39	13.25	3.20	2.86	2.58	0.24
MnO	0.22	0.74	0.31	0.11	0.25	0.16	0.09	0.57	0.39	0.34	0.14	0.10	0.37
ZnO	29.58	34.19	36.77	36.55	34.83	36.62	18.31	34.91	19.56	30.43	23.90	31.46	42.88
TiO_2	0.00	0.02	0.00	0.00	0.01	0.00	0.00	0.00	0.01	0.00	0.05	0.00	0.05
SiO_2	0.03	0.08	0.05	0.04	0.01	0.01	0.00	0.01	0.01	0.03	0.23	0.01	0.04
Total	99.74	99.91	101.3	101.39	100.68	100.42	100.2	101.44	100.17	101.44	99.82	101.72	100.63
Number of atoms in formulae (oxygen basis[4])													
Al	1.984	1.974	1.968	1.964	1.959	1.966	1.939	1.969	1.949	1.970	1.920	1.984	1.865
Fe^{3+}	0.016	0.026	0.032	0.036	0.041	0.034	0.061	0.031	0.051	0.030	0.080	0.016	0.135
Fe^{2+}	0.278	0.181	0.163	0.150	0.147	0.122	0.468	0.139	0.087	0.214	0.369	0.221	0.045
Fe_{tot}	0.294	0.207	0.195	0.186	0.188	0.156	0.529	0.170	0.138	0.244	0.449	0.237	0.180
Mg	0.073	0.047	0.030	0.059	0.102	0.080	0.167	0.105	0.536	0.139	0.127	0.112	0.011
Mn	0.006	0.019	0.008	0.003	0.006	0.004	0.002	0.014	0.009	0.008	0.004	0.002	0.010
Zn	0.651	0.760	0.814	0.804	0.766	0.811	0.395	0.760	0.392	0.655	0.526	0.676	0.997
Si	0.001	0.000	0.000	0.000	0.000	0.000	0.000	0.000	0.000	0.000	0.001	0.000	0.002
Ti	0.000	0.002	0.002	0.001	0.000	0.000	0.000	0.000	0.000	0.001	0.007	0.000	0.001
Total	3.008	3.010	3.016	3.017	3.022	3.018	3.031	3.018	3.026	3.016	3.033	3.011	3.066
Endmember calculation[3]													
Hc	27.58	17.97	16.06	14.76	14.40	12.00	45.35	13.65	8.50	21.06	35.96	21.86	4.23
Ghn	64.58	75.47	80.20	79.13	75.02	79.74	38.28	74.66	38.28	64.47	51.27	66.86	93.79
Sp	7.24	4.67	2.96	5.81	9.99	7.87	16.18	10.31	52.34	13.68	12.38	11.08	1.03
Glx	0.60	1.89	0.79	0.30	0.59	0.39	0.19	1.38	0.88	0.79	0.39	0.20	0.94

[1]Deposit: 1. Broken Hill (Australia), 2. Broken Hill (South Africa), 3. Melbourne Rockwell, 4. Mutooroo, 5. Angas, 6. Bleikvassli, 7, 8, and 9. Colorado Cu–Zn deposit, 10. Mamandur, 11. Stollberg, 12. Kvänberget, 13. Sterling Hill.
[2]Abbreviations for deposit type: BHT = Broken Hill-type, SEDEX = sedimentary exhalative, VMS = volcanogenic massive sulfide, NSZ = non-sulfide zinc.
[3]Abbreviations for spinel end members: HC = hercynite, Ghn = gahnite, Sp = spinel *sensu stricto*, Glx = galaxite.

(0.2 wt.% MgO), but the highest amount of Zn (42.9 wt.% ZnO) in gahnite from any of the deposits studied here, and generally plot outside of the metamorphosed massive sulfide compositional field 3 of Heimann et al. (2005).

3.2. Trace element chemistry

The mean, median, minimum, and maximum of the trace element concentrations of gahnite from each deposit are in Table 5, with the median concentrations being discussed hereafter. A series of box and whisker plots is presented here to facilitate comparisons between gahnite compositions in the different deposits and ore types (Fig. 3). The whisker plots show the 5th percentile, lower quartile, median, upper quartile, 95th percentile values, and outliers for concentrations of Ti, V, Cr, Mn, Co, Ni, Ga, and Cd in gahnite from each deposit.

Gahnite in SEDEX deposits contains similar amounts of V (60–87 ppm), Ni (1.4–3.2 ppm), and Cd (2.8–3.5 ppm). Gahnite from the Foster River Zn deposit contains higher concentrations of Ti (10.6 ppm), Mn (4700 ppm), Co (43 ppm), and Ga (212 ppm), and lesser amounts of Cr (29.4 ppm) than gahnite from the Angas Zn–Pb–Ag deposit (Ti = 1.8 ppm, Mn = 2270 ppm, Co = 8.7 ppm, Ga = 92 ppm, and Cr = 253 ppm).

Gahnite in BHT deposits contains 62–176 ppm V, 61–81 ppm Co, and 2.8 to 6.5 ppm Cd. Concentrations of Ga (192 ppm) and Ti (57 ppm) are, in general, higher in gahnite from Broken Hill (Australia) than in gahnite from Broken Hill (South Africa) (Ga = 135 ppm; Ti = 14 ppm), Melbourne Rockwell (Ga = 80; Ti = 20.5), and Mutooroo (Ga = 109 ppm; Ti = 2.8 ppm). Concentrations of Cr and Ni are much higher (100 and 30 ppm, respectively) in gahnite from the Melbourne Rockwell deposit than in other BHT deposits. Gahnite from Broken Hill (South Africa) contains the highest concentration of Mn (up to 4100 ppm).

The trace element concentrations of gahnite in VMS deposits are variable and not as uniform as for gahnite from BHT, NSZ, and SEDEX deposits. Concentrations of V, and to a lesser extent Mn, occur in lower amounts in gahnite from the Kvänberget deposit (0.7 ppm V and 430 ppm Mn), than in gahnite from Mamandur (V = 27.6 ppm, Mn = 2470), and some Cu–Zn deposits in Colorado. Gahnite from Mamandur contains the highest Ti content (26.2 ppm) among gahnite from VMS deposits. With the exception of this deposit, gahnite in other VMS deposits contains less than 11.5 ppm Ti and 4 ppm Ni. The Ga content of gahnite from Kvänberget (420 ppm) is higher than in gahnite from other VMS deposits (up to 182 ppm). Concentrations of Cr in gahnite from most VMS deposits are generally low (i.e., <3 ppm), with the exception of gahnite from Cu–Zn deposits in Colorado, where gahnite in anthophyllite–phlogopite rocks from the Independence deposit contains up to 257 ppm Cr. The major and trace element chemistry of gahnite in mineralogically diverse metamorphosed hydrothermal alteration zones in Colorado Cu–Zn deposits is highly variable. Assemblages in these alteration zones include, for example, cummingtonite–ilmenite–sphalerite–gahnite, gedrite–magnetite–gahnite, and anthophyllite–sillimanite–pyrite–gahnite (Heimann et al., 2005). In most of these deposits, concentrations of Ga and Co in gahnite are low, 109–400 ppm and 6.3–44 ppm, respectively, but gahnite in a gedrite–magnetite–ilmenite–pyrite–sphalerite-bearing rock from Sedalia contains anomalously high (i.e., 990–1280 ppm Ga, and 95–114 ppm Co) concentrations of these elements. The amount of Mn in gahnite from Colorado Cu–Zn deposits is variable, with concentrations ranging from 320 to 6700 ppm.

Gahnite from the Sterling Hill NSZ deposit contains relatively low concentrations of Ga (55 ppm) and Co (9 ppm), and among the highest

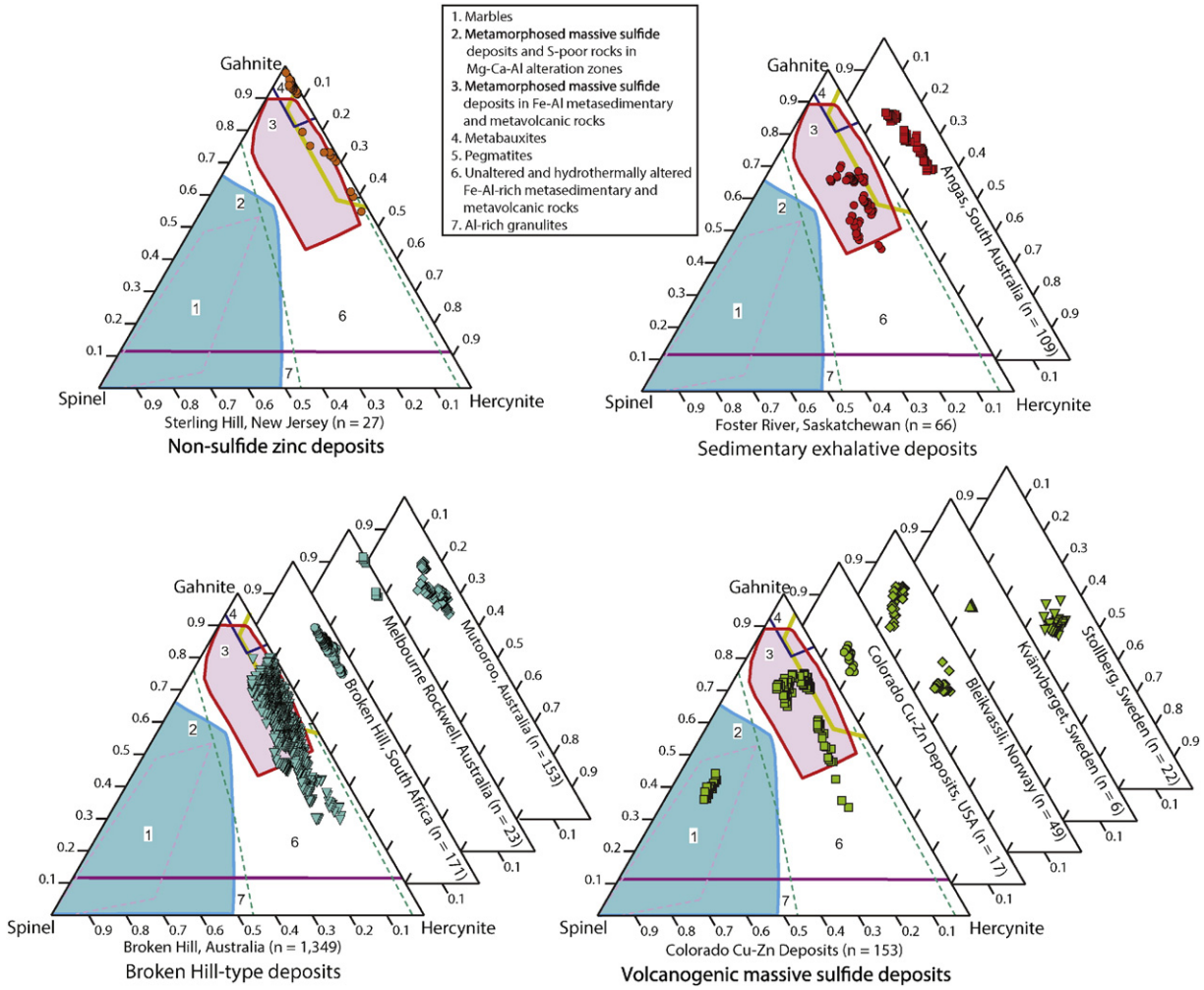

Fig. 2. Ternary plot of gahnite compositions from non-sulfide zinc, sedimentary exhalative, Broken Hill-type, and volcanogenic massive sulfide deposits in terms of the gahnite–hercynite-spinel *sensu stricto* spinel end-members. Numbers correspond to compositional ranges of gahnite from different geological settings as defined by Heimann et al. (2005). 1. Marbles; 2. Metamorphosed massive sulfide deposits and S-poor rocks in Mg–Ca–Al alteration zones; 3. Metamorphosed massive sulfide deposits in altered Fe–Al metasedimentary and metavolcanic rocks; 4. Metabauxites; 5. Pegmatites; 6. Unaltered and hydrothermally altered Fe–Al-rich metasedimentary and metavolcanic rocks; 7. Al-rich granulites. The number of analyses obtained from each location is given in brackets.

concentrations of Ti (218 ppm), Cr (278 ppm), and Cd (25.1 ppm) for gahnite analyzed herein.

4. Discussion

The chemical compositions of gahnite for each deposit type are variable, and for several elements they overlap, and do not uniquely define a compositional range for a specific deposit type (Fig. 3). However, when some elements are used in combination with others they lend themselves to the development of compositional plots capable of distinguishing and classifying gahnite from different deposit types. Gahnite in the Sterling Hill deposit contains high concentrations of Ti, V, Cr, Zn, Cd, and low amounts of Mg, Al, Co, and Ga, and is distinguished from that in BHT, SEDEX, and VMS deposits in plots of Co versus Cd (Fig. 4A) and Al versus Mg (Fig. 4B). High concentrations of Ti, V, Co, Ni, and low amounts of Mg, are typical of gahnite in BHT deposits, which can be discriminated from gahnite in SEDEX and VMS deposits in plots of Mg versus V (Fig. 4C), and Co versus V, respectively (Fig. 4D). However, some Co- and V-rich gahnite from Colorado Cu–Zn deposits (i.e., Bon Ton, Cotopaxi, Independence, and Sedalia) compositionally overlap gahnite from BHT deposits.

Gahnite in SEDEX deposits contains low concentrations of Ti, Co, Ni, and Ga, and high quantities of Mg, V, Cr, Mn, and Zn. Most gahnite in VMS deposits contains low amounts of V, Cr, Mn and Co, and high concentrations of Mg, Ti, and Ga. Thus, plots of Mn versus Ti (Fig. 4E), and Co versus Ti serve to distinguish gahnite in SEDEX deposits from that in a VMS deposit (Fig. 4F). However, the composition of gahnite in some Colorado Cu–Zn deposits plot within the SEDEX field. It is noted that the major element compositions of gahnite from central Colorado is the most variable of any gahnite district yet reported (i.e., gahnite-, hercynite- and spinel-rich compositions, Heimann et al., 2005, Fig. 4, p. 611). This is in large part due to the unusually Mg-rich alteration, which commonly contains gahnite, compared to other VMS deposits. Although additional compositions of gahnite from other VMS and SEDEX districts need to be obtained, it may be that the unusual gahnite-bearing assemblages in the central Colorado district result in compositions that are atypical for gahnite from VMS deposits, which plot within the SEDEX field of Fig. 4E and F. In addition to compositional distinctions shown in Fig. 4E and F, which are based on Co versus Ti, and Mn versus Ti, respectively, the compositions of gahnite from SEDEX deposits also generally contain higher concentrations of Cr and V than gahnite from VMS deposits (Fig. 3). Note that compositions of gahnite from BHT and NSZ deposits are not included in Fig. 4E and F because

Table 5
Trace element compositions of gahnite from different types of metamorphosed ore deposits.[a]

		SEDEX		BHT				VMS					NSZ
		Angas	Foster River	Broken Hill, South Africa	Broken Hill, Australia	Melbourne Rockwell	Mutooroo	Bleikvassli	Colorado Cu–Zn Deposits	Mamandur	Kvänberget	Stollberg	Sterling Hill
		(n = 10)	(n = 56)	(n = 56)	(n = 606)	(n = 20)	(n = 55)	(n = 19)	(n = 100)	(n = 34)	(n = 3)	(n = 10)	(n = 70)
Li	Mean	4.0	28	14.1	6.4	0.98	5.0	7.5	1.60	1.85	1.28	3.0	2.39
	Med	3.9	29	11.4	4.9	0.71	5.0	7.7	1.14	1.87	1.28	3.0	2.03
	Min	2.33	10.5	4	0.52	0.41	1.85	3.8	0.31	0.83	1.13	2.47	0.42
	Max	5.9	53	32	28.5	2.93	10.5	10.9	4.5	2.7	1.42	3.5	6.1
Ti	Mean	2.03	12.4	17.6	64	65	10.7	5.7	26.3	31	1.68	9.6	212
	Med	1.75	10.6	14.2	57	20.5	2.77	5.3	11.5	26.2	1.69	9.2	218
	Min	0.74	3.0	5.8	0.50	9.0	0.86	1.32	1.13	14.9	1.04	7.8	4.4
	Max	3.5	36	52	630	880	43	16.5	102	77	2.32	14.7	436
V	Mean	84	85	109	199	177	118	5.4	38	43	0.65	1.66	136
	Med	87	60	62	148	176	133	5.6	25.1	27.6	0.74	1.48	141
	Min	58	27.3	9.8	0.160	149	45	2.66	0.98	15.2	0.31	0.84	76
	Max	114	470	380	1010	195	194	8.7	144	112	0.91	2.53	210
Cr	Mean	219	123	124	257	107	65	5.9	26.5	5.4	b.d.	3.7	256
	Med	253	29.4	11	59	100	6.7	2.78	2.26	2.63	b.d.	3.6	278
	Min	30	1.80	0.47	0.08	40	0.67	0.77	0.45	0.51	b.d.	2.24	77
	Max	460	1140	740	6400	186	490	22.9	257	31	b.d.	6.2	450
Mn	Mean	2360	5500	4400	1320	2070	930	1110	2770	2640	430	1020	3700
	Med	2270	4700	4100	1140	2070	840	1070	2470	2460	430	1030	3700
	Min	1840	2890	3400	247	1510	370	560	320	1800	400	780	1490
	Max	3100	12300	6100	5280	2550	1690	1620	6700	3800	462	1240	5800
Co	Mean	10.6	61	59	91	65	64	8.4	26.9	17.4	2.43	2.29	8.7
	Med	8.7	43	61	81	68	65	7.8	15.5	17.3	2.36	2.35	8.7
	Min	7.9	18.8	18.9	12.1	45	39	0.52	6.3	14.2	2.31	1.73	5.7
	Max	16.6	165	112	273	73	109	20.1	114	22.0	2.62	2.68	14.5
Ni	Mean	1.63	6.0	3.7	29.3	34.2	11.5	1.33	3.9	51	0.62	0.58	11.9
	Med	1.37	3.2	3.6	12	29.9	6.6	1.14	3.9	53	0.62	0.58	10.2
	Min	0.56	1.42	2.00	0	25	0.80	0.35	0.06	42	0.62	0.58	4.4
	Max	3.0	44	10.6	235	48	28.4	2.72	9.6	62	0.62	0.58	29
Ga	Mean	108	277	137	227	85	113	113	286	174	380	144	58
	Med	92	212	135	192	80	109	108	182	141	420	144	55
	Min	62	94	76	68	62	84	94	109	124	292	114	42
	Max	173	710	244	570	105	167	168	1280	249	440	169	78
Cd	Mean	3.5	3.0	2.76	4.2	8.1	5.0	4.7	4.3	4.2	4.7	1.39	26.3
	Med	3.5	2.76	2.77	3.4	6.5	4.7	3.8	4.1	3.4	4.6	1.24	25.1
	Min	2.09	1.12	1.06	0.39	3.1	2.23	1.97	0.95	1.96	4.3	0.88	5.9
	Max	4.8	6.3	5.6	26.1	15.7	12.7	10.5	10.7	11.3	5.1	2.40	69

Notes.
[a] Concentrations of Li, Ti, V, Cr, Mn, Co, Ni, and Cd are reported in ppm; BHT = Broken Hill-type deposit; SEDEX = sedimentary exhalative deposit; VMS = volcanogenic massive sulfide deposit; NSZ = non-sulfide zinc deposit; b.d. = below detection limits.

they are distinguished from gahnite derived from SEDEX and VMS deposits in Fig. 4A–D.

It is stressed here that while there is overlap in composition in several trace elements for different deposits, as illustrated by the whisker plots in Fig. 3, Fig. 5 uses a tree diagram for specific elements shown in Fig. 4 to allow the composition of gahnite in the four types of metamorphosed ore deposits to be distinguished. Compositions of unknown detrital gahnite should first be plot in Fig. 4A (Co vs. Cd) and B (Al vs. Mg) to discriminate non-sulfide zinc deposits from the other three types of deposit. Thereafter, unknown samples should be plot in Fig. 4C (Mg vs. V) and D (Co vs. V) to distinguish BHT deposits from VMS and SEDEX deposits. The last two deposit types are subsequently discriminated using Fig. 4E (Co vs. Ti) and F (Mn vs. Ti).

Although the reasons why major and trace element compositions of minerals vary in a given deposit have been discussed elsewhere, the conditions affecting the major element chemistry of gahnite include fO_2, fS_2, temperature, pressure conditions, and host rock geochemistry (e.g., Heimann et al., 2005; Shulters and Bohlen, 1989; Spry and Scott, 1986). Experiments by Spry and Scott (1986) showed that the major element composition of zincian spinel in the gahnite–hercynite solid solution is strongly dependent upon fS_2 and fO_2, which are dictated by the *a*FeS content of coexisting Fe-bearing sulfides (i.e., sphalerite, pyrite, and pyrrhotite). The composition of gahnite in the gahnite–hercynite solid solution is buffered and fixed (i.e., ~65–85 mol% $ZnAl_2O_4$), where coexisting Fe-bearing sulfides comprise more than ~1 vol.% of the modal abundance of the host rock lithology, over the broad range of gahnite stability (i.e., upper greenschist to granulite facies) in metamorphic rocks (Spry and Scott, 1986; Spry and Teale, 2009). Because gahnite in BHT, SEDEX, and VMS deposits commonly coexists with Fe and Zn sulfides, the gahnite:hercynite ratio overlaps, such that the provenance of detrital grains cannot be distinguished solely on the basis of major element chemistry. However, the Sterling Hill NSZ deposit contains only trace amounts of sphalerite and Fe-sulfides, and, as a result, the gahnite:hercynite ratio was never buffered by the *a*FeS content of coexisting Fe-bearing sulfides (i.e., sphalerite, pyrite, and pyrrhotite). The high Zn content of gahnite at Sterling Hill is a function of the high bulk-rock Zn content, as indicated by the presence of zincite (ZnO), willemite (Zn_2SiO_4), and franklinite ($ZnFe_2O_4$) that dominate the ore (Johnson et al., 1990).

Gahnite in VMS and SEDEX deposits is more Mg-rich than that in BHT and the Sterling Hill NSZ deposit. The spinel *sensu stricto* component does not take part in gahnite-forming desulfidation reactions; therefore, enrichment in Mg content is related to host rock geochemistry. Gahnite-bearing samples from the Colorado Cu–Zn deposits were obtained mostly from metamorphosed Mg-rich hydrothermal alteration zones. Heimann et al. (2005) showed that Mg-rich gahnite in these deposits coexists with other Mg-rich phases (e.g., anthophyllite, phlogopite, gedrite, diopside, and hornblende), whereas gahnite,

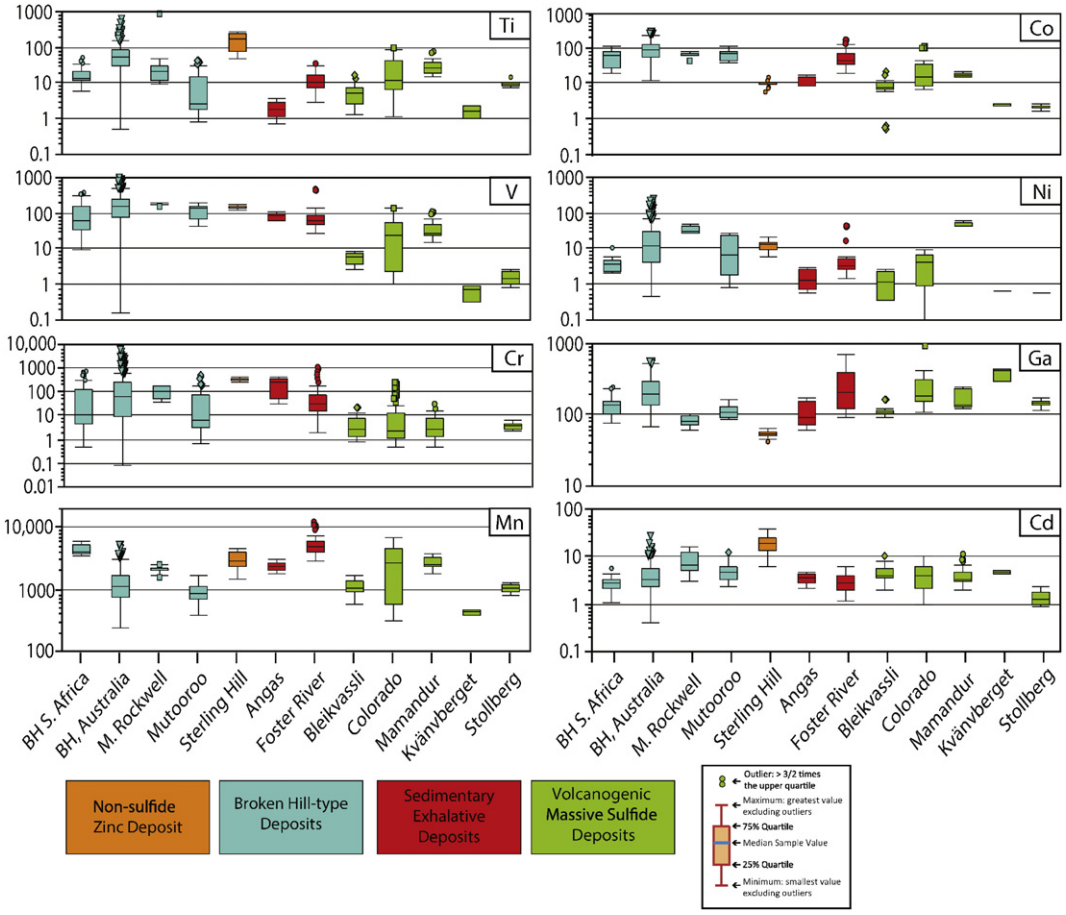

Fig. 3. Box and whisker plots for the elements Ti, V, Cr, Mn, Co, Ni, Ga, and Cd grouped on the basis of each deposit and colored based on deposit type. Concentrations of elements are in ppm and plotted on a logarithmic scale. The edges of whiskers represent the 5th percentile (bottom) and 95th percentile values (top), the edges of the box represent the lower quartile and upper quartile (50th percentile), and the solid line across the box represents the median. Outliers are shown as disconnected points.

which is enriched in Fe and/or Zn coexists with Fe-rich silicates (e.g., almandine, biotite).

Gahnite in the Sterling Hill NSZ deposit contains the lowest concentrations of Al, because of the substitution of Fe^{3+} into the octahedral structural site, which is filled normally by Al in aluminous spinels. Elevated amounts of the franklinite ($ZnFe_2O_4$) component in zincian spinel from Sterling Hill occurs where gahnite is in contact with franklinite or as exsolutions in franklinite (Carvalho and Sclar, 1988). These elevated Fe^{3+} concentrations indicate that gahnite at Sterling Hill formed under more oxidizing conditions than gahnite in samples that were analyzed here from BHT, SEDEX, and VMS deposits.

Factors influencing the trace element chemistry of gahnite are unknown and are not fully evaluated here due to the absence of experimental studies, but likely include whole rock geochemistry, partitioning of trace elements between gahnite and other minerals in the matrix, temperature, pressure, fO_2, fS_2, fH_2O, crystal-chemical controls (i.e., the major element chemistry of gahnite), and the composition of precursor minerals (e.g., sphalerite, garnet, pyrrhotite). Although numerous empirical and experimental studies have been done to examine the incorporation of trace elements into magnetite (see Nadoll et al., 2014), zincian spinels have received little attention, with the exception of an empirical study on the partitioning of trace elements between gahnite and coexisting biotite and garnet (O'Brien et al., 2013). As a result, it is difficult to speculate on how changes in physicochemical conditions (i.e., temperature, pressure, fO_2, fS_2, fH_2O) affect the trace element chemistry of gahnite without well-constrained experimental studies. But it is likely that incorporation of redox sensitive elements, such as Cr and V, is dependent on oxygen fugacity (e.g., substitution of V^{3+} into gahnite is compatible; whereas V^{5+} is likely incompatible).

The focus of this paper is to determine whether the discrimination tree diagram can be used to compositionally distinguish gahnite among the four different ore types discussed here. However, we briefly speculate on some of the factors likely responsible for the variability in trace element compositions. A first-order control on the available trace element budget during gahnite growth is the bulk rock geochemistry of its host. Although the BHT, SEDEX, NSZ, and VMS deposits examined in this study formed in extensional rift settings, they occur in different parts of the rift and in different host rocks. Therefore, factors affecting concentrations of the first series transition metals, Ga, and Cd in the protolith of gahnite-bearing rocks will influence gahnite chemistry.

Gahnite in BHT deposits contains elevated concentrations of Ti, V, Co, and Ni, and low Mg contents. Deposits of this type occur in a sequence of amphibolites, and metasedimentary, metavolcanic, and metaintrusive rocks (e.g., Walters, 1998). At Broken Hill, Australia, sulfide mineralization, with attendant gahnite-bearing rocks, locally occurs in the Hores Gneiss and the Potosi Gneiss, but it is also spatially related to mafic igneous rocks. These rocks form part of a group of bimodal volcanic rocks that have rhyodacite–tholeiitic affinities (Johnson and Klingner, 1975; Raveggi et al., 2007, 2008). Variability in the nature of the metasedimentary rocks (i.e., metapelite, metapsammites, and metapsammopelite) is likely a function of sediment provenance, input of detrital minerals, presence of hydrothermal or chemical sediments, and seawater chemistry. The mixed metasedimentary and tholeiitic

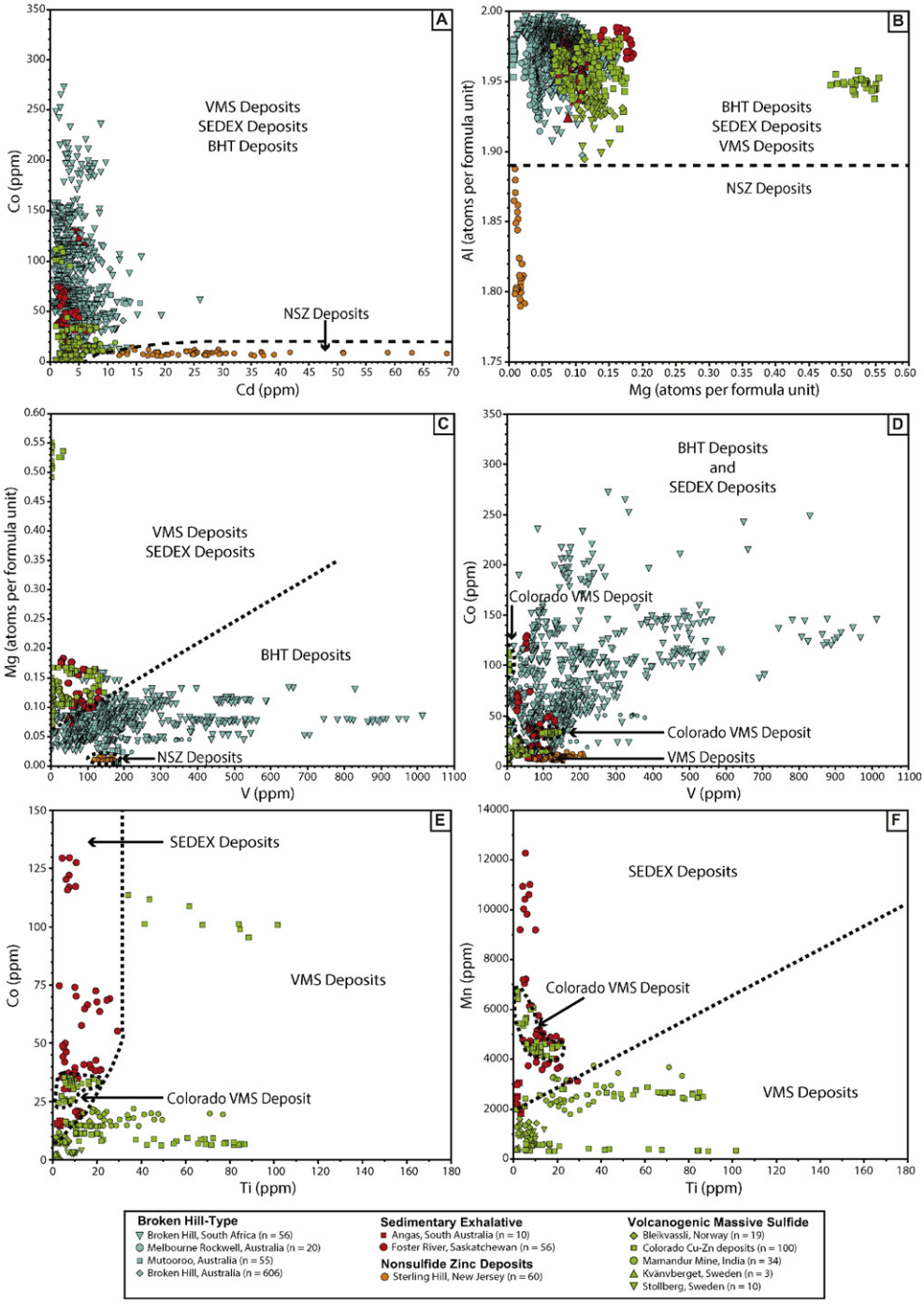

Fig. 4. Compositions of gahnite from various types of metallic mineral deposits in a series of bivariate plots: A. Co (ppm) versus Cd (ppm); B. Al (atoms per formula unit) versus Mg (atoms per formula unit); C. Mg (atoms per formula unit) versus V (ppm); D. Co (ppm) versus V (ppm); E. Co (ppm) versus Ti (ppm); F. Mn (ppm) versus Ti (ppm).

contributions to the Hores and Potosi Gneisses, and the processes by which they formed may account for the high concentrations of V and Ti, but low Mg, Cr, and Ni contents of gahnite. The higher proportion of mafic igneous rocks to felsic rocks at Melbourne Rockwell relative to Broken Hill, likely contributed to the difference in trace element content of gahnite between the two locations. However, gahnite in most BHT deposits, including Broken Hill, Australia, occurs predominantly in exhalative/inhalative chemical sedimentary rocks. The concentrations of transition metals in such rocks have been used in the past to assess the relative contribution of hydrothermal (e.g., Mn, Zn, Cr, Cd), hydrogenous (e.g., Mg, V, Co, Ni), and detrital (e.g., Cr, Ti) components to the protolith (e.g., Bonatti, 1975; Heimann et al., 2011; Hein et al., 2005). Although Cr is generally not considered an element that is enriched in hydrothermal fluids, Arai and Akizawa (2014) showed that Cr in high-temperature hydrothermal solutions may be more elevated. However, its behavior in lower temperature hydrothermal fluids (i.e., temperatures associated with exhalations from metal-bearing hydrothermal vents) remains unclear. In certain cases, Mg, Co, Ni, and Ti could also be considered hydrothermal, enriched either by fluid transport or, in the case of Ti, by leaching. Elevated concentrations of Co, V, and Ni in gahnite from BHT deposits indicate a strong hydrogenetic input whereas elevated concentrations of Ti likely indicates a detrital

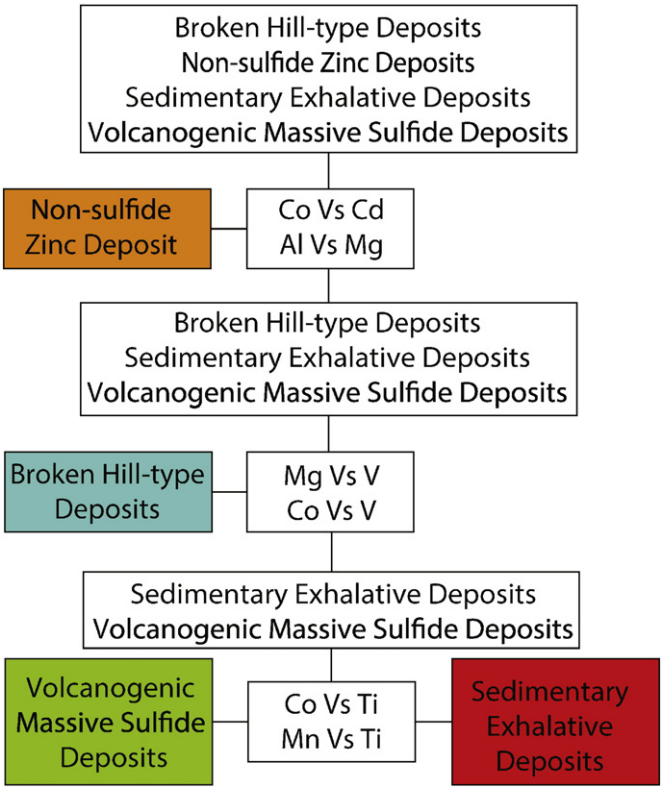

Fig. 5. Schematic diagram showing the classification of different deposit types using a series of bivariate plots of gahnite chemistry (major and trace elements). The type of metamorphosed ore deposit from which gahnite was derived if found in an unconsolidated sediment can be determined using the six bivariate plots in Fig. 4. Compositions should first be plot in Fig. 4A and B to distinguish non-sulfide zinc deposits from the three other deposit types. Subsequently, plotting the compositional data for gahnite from these three remaining deposits in Fig. 4C and D, allows for gahnite from Broken Hill-type deposits to be identified. Gahnite in volcanogenic massive sulfide deposits and sedimentary exhalative deposits can then be distinguished from one another in Fig. 4E and F.

component. Gahnite in BHT deposits contains the highest median concentrations of V and Co for gahnite analyzed in this study. Vanadium is adsorbed and scavenged by Fe-oxide particles from hydrothermal plumes, resulting in the concentration of this element in exhalative sediments distal to the vent (Krauskopf, 1956; Trefry and Metz, 1989).

Distribution coefficients were determined by O'Brien et al. (2013) for gahnite–biotite and gahnite–garnet pairs in the Broken Hill domain, Australia, to assess how the partitioning of elements between gahnite and coexisting minerals affect gahnite chemistry. Distribution coefficients for gahnite–biotite pairs suggest Cr, Ga, Co, Cd, Ni, and to a lesser extent V, preferentially partition into gahnite, and Li and Ti partition into biotite, whereas for gahnite–garnet pairs Ni, Ga, Cr, V, Co, and Li partition more strongly into gahnite, and Ti, Cd, and Mn partition into garnet. Because transition metals preferentially partition into gahnite, the presence of biotite (except for Li and Ti) and garnet (except for Mn, Ti, and Cd) will not greatly affect the concentrations of V, Cr, Co, Ni, and Ga in gahnite. In the Broken Hill deposit (Australia), gahnite most commonly occurs in blue quartz–gahnite lode rocks, which can also contain trace amounts of a variety of accessory minerals (e.g., apatite, galena, orthoclase, sphalerite, tourmaline, and trace magnetite, sillimanite, rutile, and titanite) (Barnes et al., 1983). Because of the paucity of these accessory minerals, competition for the incorporation of trace elements in accessory minerals is likely low, which results in the enrichment of Ti, V, Ni, and Co in gahnite. However, one exception is blue quartz, which is mostly deficient in transition elements, but is saturated in Ti because it generally contains rutile needles (e.g., Seifert et al., 2011). Where present, titanite is rare by comparison to gahnite and was not observed in contact with gahnite in samples studied here. In a preliminary attempt to evaluate crystal-chemical controls on the trace element composition of gahnite, the major element compositions of gahnite were plotted as a function of trace element compositions. Given that all major-trace element pairs had r^2 values less than 0.2, it is likely that the crystal-chemical controls on trace element contents are minimal.

Gahnite in SEDEX deposits contains low concentrations of Ti, Co, Ni, and Ga, and high amounts of Zn, Mg, Cr, and V. The Angas deposit occurs in a sequence of metasedimentary rocks with metagreywacke predominating over metapelite, whereas metapsammite, metapelite, meta-quartzite, and meta-arenite are spatially associated with the Foster River prospect. Volcanic rocks, including volcaniclastic rocks, appear to be absent from the stratigraphic sequence hosting both of these occurrences, although their presence cannot be ruled out. Gahnite-bearing sulfide mineralization at the Foster River prospect occurs in sulfidic-quartzite rocks (i.e., K-feldspar-biotite–sillimanite–graphite rocks with accessory magnetite, garnet, and tourmaline) (Steadman and Spry, 2015). Concentrations of V in sedimentary rocks are sensitive to redox conditions and are highest in organic-rich black shales. The spatial association of graphitic schists to graphite–gahnite-bearing sulfides at Foster River likely accounts for the elevated V content of gahnite. Chromium can either accumulate in sediments by adsorption onto Fe-oxides from seawater (like V) or through the deposition of detrital components (Murray et al., 1983), and this may be the reason for its high concentration in gahnite from Foster River.

Using the classification scheme of Franklin et al. (2005) for VMS deposits, the Stollberg, Kvänberget, and Cu–Zn deposits in Colorado share characteristics with bimodal felsic-type deposits, whereas Mamandur is a bimodal-mafic deposit. Compositional variability for gahnite from VMS deposits is greater than for gahnite from BHT and SEDEX deposits. This is, in large part, likely related to the proximity and abundance of mafic igneous rocks to VMS deposits, which tend to contain higher amounts of transition elements than felsic rocks.

Gahnite in VMS deposits contains high concentrations of Ti, Ga, Mg, and low concentrations of V, Co, and Cr. Gahnite samples studied here are from metamorphosed hydrothermally altered felsic volcanic rocks or massive sulfides (e.g., Heimann et al., 2005). Concentrations of transition metals in volcanic rocks generally decrease with increasing melt fractionation and with increasing silica content in magma because of the crystallization of mafic minerals (e.g., olivine, pyroxene), Fe–Ti oxides and immiscible sulfides, which potentially accounts for the low concentrations of Cr, V, and Co in gahnite in metamorphosed felsic volcanic rocks (Ridley, 2012; Stanton, 1994). Hydrothermal alteration associated with fluid–rock interaction during the emplacement of ore minerals likely influenced the concentrations of some transition metals in the protolith of gahnite-bearing rocks. During hydrothermal alteration, Al, Ti, V, and Cr are generally immobile, whereas Mn, Co, and Ni are considered mobile (Humphris and Thompson, 1978; Piercey, 2009). Gahnite in metamorphosed alteration zones associated with VMS deposits is commonly intergrown with a variety of ferromagnesian silicates (e.g., amphiboles, biotite, garnet), sulfides (e.g., sphalerite, pyrrhotite), and oxides (e.g., magnetite, ilmenite). Therefore, it is likely that the trace element content of gahnite will also be variable and may be a function of partition of trace elements between coexisting phases, because coexisting silicates and oxides can accommodate transition metals (e.g., Nehring et al., 2010).

Given the debate concerning the origin of two deposits, Bleikvassli (i.e., SEDEX versus VMS) and Stollberg (i.e., is it a VMS deposit?), the compositions of gahnite from these locations were used as test cases and applied to the discrimination tree diagram. The composition of gahnite from the Stollberg samples (n = 10, Ti = 7.8 to 14.7 ppm; Mn = 780 to 1240 ppm; Co = 1.73 to 2.68 ppm) fall within the VMS fields in Fig. 4E and F, whereas those for Bleikvassli (n = 19; Ti = 1.32 to 16.5 ppm; Mn = 320 to 670 ppm; Co = 0.52 to 20.1 ppm) drape the SEDEX-VMS fields in Fig. 4E and fall within the VMS field in

Fig. 4F. These data are few in number and several more data need to be obtained to statistically verify whether the compositions of gahnite from these two locations are consistent with the proposed VMS affiliations, which were based on geological and geochemical considerations.

The Franklin Marble, a prominent carbonate unit in the Reading Prong of New Jersey, hosts the Sterling Hill NSZ deposit (Johnson et al., 1990; Metsger, 2001). Gahnite from this deposit contains the highest concentrations of Cd of any gahnite analyzed here. Trace element studies of sphalerite by Cook et al. (2009) showed that sphalerite can contain high concentrations of Cd (up to 10,000 ppm). Sphalerite constitutes only a trace component of the ore at Sterling Hill. Although distribution coefficients have not been determined for gahnite–sphalerite pairs, preferential partitioning of Cd into gahnite in the absence of sphalerite and other sulfides may have produced the elevated concentrations of Cd in gahnite from Sterling Hill.

5. Summary and conclusions

The gahnite classification tree diagram serves as a way to determine the provenance of detrital gahnite based on their major and trace element composition. Additional analysis of the chemistry of gahnite in metamorphosed sulfide and non-sulfide deposits will undoubtedly refine the limits of the compositional fields identified here. However, based on the data obtained here the main conclusions of this study are:

1) The trace element chemistry of gahnite in BHT, NSZ, SEDEX, and VMS deposits is dominated by Ti, V, Cr, Mn, Co, Ni, Ga, and Cd.
2) Using the gahnite classification tree diagram, gahnite in NSZ deposits can be discriminated from gahnite in BHT, SEDEX, and VMS deposits on the basis of plots of Co versus Cd, and Al versus Mg. Gahnite in BHT deposits can subsequently be distinguished from that in SEDEX and VMS deposits based on plots of Mg versus V, and Co versus V, whereas the composition of gahnite in SEDEX deposits is distinct from that in VMS deposits based on plots of Mn versus Ti, and Co versus Ti.
3) The trace element composition of gahnite depends on a variety of physicochemical parameters as well as the bulk rock composition and trace element partitioning between gahnite and coexisting minerals. However, the relative importance of these parameters is unknown, although it is likely that the bulk chemistry of the rock hosting gahnite and trace element partitioning between gahnite and coexisting oxides and ferromagnesian silicates have a major effect on the composition of gahnite. In contrast, it is also likely that crystal-chemical controls of trace element compositions of gahnite are minimal.
4) The composition of gahnite can be used as an exploration guide to metamorphosed massive sulfide and non-sulfide deposits in productive ore camps and in greenfield terranes, where it can occur as a resistate mineral in unconsolidated sediments.

Acknowledgments

A Hugo Dummett Fund Research Grant to JJO from the Society of Economic Geologists and an Iowa State University Incentive Grant to PGS provided funding for this project. We thank Ellery Frahm, Anette von der Handt, and Fred Davis for assistance with electron microprobe analyses. Assistance from Angela Zhang through the REAP summer internship program at Iowa State University is also appreciated. We also thank Kate Frank for collecting trace element data on gahnite from the Sterling Hill deposit and Andy Tomkins for evaluating an earlier draft of this manuscript. Maria Boni and Magnus Ripa are sincerely thanked for their constructive and helpful reviews of this paper.

References

Allen, R.L., Lundstrom, I., Ripa, M., Christofferson, H., 1996. Facies analysis of a 1.9 Ga, continental margin, back-arc, felsic caldera province with diverse Zn–Pb–Ag–(Cu–Au) sulfide and Fe oxide deposits, Bergslagen region, Sweden. Econ. Geol. 91, 979–1008.
Arai, S., Akizawa, N., 2014. Precipitation and dissolution of chromite by hydrothermal solutions in the Oman ophiolite: new behavior of Cr and chromite. Am. Mineral. 99, 28–34.
Aubrecht, R., Méres, S., Sýkora, M., Mikuš, T., 2009. Provenance of the detrital garnets and spinels from the Albian sediments of the Czorsztyn Unit (Pieniny Klippen Belt, Western Carpathians, Slovakia). Geol. Carpath. 60, 463–483.
Averill, S.A., 2001. The application of heavy indicator mineralogy in mineral exploration with emphasis on base metal indicators in glaciated metamorphic and plutonic terrains. In: McClenaghan, M.B., Bobrowsky, P.T., Hall, G.E.M., Cook, S.J. (Eds.), Drift Exploration in Glaciated Terrains. Geological Society, London, Special Publications 185, pp. 69–81.
Averill, S.A., 2007. Recent advances in base metal indicator mineralogy: an update from Overburden Drilling Management Limited. EXPLORE, Newsletter for the Association of Applied Geochemists 134 pp. 2–6.
Averill, S.A., 2011. Viable indicator minerals in surficial sediments for two major base metal deposit types: Ni–Cu–PGE and porphyry Cu. Geochem. Explor. Environ. Anal. 11, 279–291.
Barnes, R.G., 1988. 1. Styles of mineralization in the Broken Hill block, 2. mineral deposits of the southwestern Broken Hill Block: metallogenic studies of the Broken Hill and Euriowie Blocks, New South Wales. Bull. Geol. Surv. NSW 32 (1 and 2) (250 pp.).
Barnes, R.G., Stevens, B.P.J., Stroud, W.J., Brown, R.E., Willis, I.L., Bradley, G.M., 1983. Zinc-, manganese-, and iron-rich rocks and various minor rock types. Rec. Geol. Surv. NSW 21, 289–323.
Bartholomaeus, M.A., 1987. Mineral deposits of the Rockwell 1:25,000 sheet area, Broken Hill. Geological Survey of New South Wales. Unpublished Report, GS1987/068.
Bjerkgård, T., 1999. Metal distribution and formation of the Bleikvassli Zn–Pb–(Cu) deposit, Nordland, Norway. In: Stanley, et al. (Eds.), Mineral Deposits: Processes to Processing. Balkema, Rotterdam, pp. 931–934.
Bonatti, E., 1975. Metallogenesis at oceanic spreading centers. Ann. Rev. Earth Planet. Sci. 3, 401–431.
Both, R.A., McElhinney, R., Toteff, S., 1995. The Angas Zn–Pb–Ag deposit in the Kanmantoo Group, South Australia: synsedimentary or metamorphic? In: Pasava, J., Kríbek, B., Zák, K. (Eds.), Mineral Deposits: From Their Origin to Their Environmental Impacts. A.A. Balkema, Rotterdam, pp. 847–850
Burton, G.R., 1994. Metallogenic studies of the Broken Hill and Euriowie Blocks, New South Wales. 3. Mineral deposits of the South Eastern Broken Hill Block. Bull. Geol. Surv. NSW 32 (100 pp.).
Carvalho, A.V., Sclar, C.B., 1988. Experimental determination of the ZnFe2O4–ZnAl2O4 miscibility gap with application to franklinite–gahnite exsolution intergrowths from the Sterling Hill zinc deposit, New Jersey. Econ. Geol. 83, 1447–1452.
Chattopadhyay, P.K., 1999. Zn-spinel in the metamorphosed Zn–Pb–Cu sulphide deposit at Mamandur, southern India. Mineral. Mag. 63, 743–755.
Cook, N.J., 1993. Conditions of metamorphism estimated from alteration lithologies and ore at the Bleikvassli Zn–Pb–(Cu) deposit, Nordland, Norway. Nor. Geol. Tidsskr. 73, 226–233.
Cook, N.J., Spry, P.G., Vokes, F.M., 1998. Mineralogy and textural relationships among sulphosalts and related minerals in the Bleikvassli Zn–Pb–(Cu) deposit, Nordland, Norway. Mineral. Deposita 34, 35–56.
Cook, N.J., Ciobanu, C.L., Pring, A., Skinner, W., Shimizu, M., Danyushevsky, L., Saini-Eidukat, B., Mecher, F., 2009. Trace and minor elements in sphalerite: a LA-ICP-MS study. Geochim. Cosmochim. Acta 73, 4761–4791.
Coombe, W., 1994. Sediment-hosted base metal deposits of the Wollaston domain, northern Saskatchewan. Saskatchewan Energy and Mines Report 213 (128 pp.).
Crabtree, D.C., 2003. Preliminary results from the James Bay lowland indicator mineral sampling program. Ont. Geol. Surv. Open File Rep. 6108 (115 pp.).
Drake, A.A., 1990. The regional geologic setting of the Franklin–Sterling Hill district, *in* Character and origin of the Franklin–Sterling Hill orebodies. Lehigh University–Franklin–Ogdensburg Mineralogical Society Symposium, Proceedings Volume, Bethlehem, PA, pp. 14–31.
Dupuis, C., Beaudoin, G., 2011. Discriminant diagrams for iron oxide trace element fingerprinting of mineral deposit types. Mineral. Deposita 46, 319–335.
Frank, K.S., Spry, P.G., Raat, H., Allen, R.S., Jansson, N., O'Brien, J.J., 2014. Variability in the geological and geochemical setting and mineral chemistry of metamorphosed base metal sulfide deposits in the Stollberg ore field, Sweden. Society of Economic Geologists SEG 2014 Conference, Keystone, Colorado, Abstract 0393-00042.
Franklin, J.M., Gibson, H.L., Galley, A.G., Jonasson, I.R., 2005. Volcanogenic massive sulfide deposits. Economic Geology 100th Anniversary Volume (523–560 pp.).
Ghosh, B., Some, S., Thakur, A., 2011. Petrogenesis of zincian spinel from Mamandur base metal sulphide prospect, Tamil Nadu. J. Geol. Soc. India 78, 365–369.
Greenfield, J., 2003. A critical review of Broken Hill ore system models. Commonw. Sci. Ind.l Res. Organ. Explor. Rep. 1160R (192 pp.).
Gurney, J.J., 1984. A correlation between garnets and diamonds. In: Glover, J.E., Harris, R.G. (Eds.), Kimberlite Occurrences and Origin: A Basis for Conceptual Models in Exploration. Geology Department and University Extension, University of Western Australia Publication 8, pp. 143–166.
Gustafson, L.B., Williams, N., 1981. Sediment-hosted stratiform deposits of copper, zinc, and lead. Society of Economic Geologists 75th Anniversary Volumepp. 139–178.
Hallberg, A., Bergman, T., Gonzalez, J., Larsson, D., Morris, G.A., Perdahl, J.A., Ripa, M., Niiranen, T., Eilu, P., 2012. Metallogenic areas in Sweden: geological survey of Finland. Spec. Pap. 53, 139–206.

Haydon, R.W., McConachy, G.W., 1987. The stratigraphic setting of the Broken Hill Pb–Zn–Ag mineralization at Broken Hill. Econ. Geol. 82, 826–856.
Heimann, A., Spry, P.G., Teale, G.S., 2005. Zinc-rich spinels associated with Proterozoic base metal sulfide occurrences, Colorado, and their use as guides to metamorphosed massive sulphide deposits. Can. Mineral. 43, 601–622.
Heimann, A., Spry, P.G., Teale, G.S., 2011. Chemical and crystallographic constraints on the geochemistry of garnet in garnet-rich rocks, southern Proterozoic Curnamona Province, Australia. Mineral. Petrol. 101, 49–74.
Hein, J.R., Koschinsky, A., McIntyre, B.R., 2005. Mercury- and silver-rich ferromanganese-oxides, southern California borderland. Deposit model and environmental implications. Econ. Geol. 100, 1151–1168.
Hicken, A.K., McClenaghan, M.B., Layton-Matthews, D., Paulen, R.C., Averill, S.A., Crabtree, D., 2013a. Indicator mineral signatures of the Izok Lake Zn–Cu–Pb–Ag-volcanogenic massive sulphide deposit, Nunavut: part 1 bedrock samples. Geol. Surv. Can. Open File Rep. 7173 (107 pp.).
Hicken, A.K., McClenaghan, M.B., Paulen, R.C., Layton-Matthews, D., Averill, S.A., Crabtree, D., 2013b. Indicator mineral signatures of the Izok Lake Zn–Cu–Pb–Ag-volcanogenic massive sulphide deposit, Nunavut: part 2 till. Geol. Surv. Can. Open File Rep. 7173 (107 pp.).
Humphris, S.E., Thompson, G., 1978. Trace element mobility during hydrothermal alteration of oceanic basalts. Geochim. Cosmochim. Acta 42, 127–136.
Jansson, N.F., Erismann, F., Lundstam, E., Allen, R.L., 2013. Evolution of the Paleoproterozoic volcanic–limestone–hydrothermal sediment succession and Zn–Pb–Ag and iron oxide deposits at Stollberg, Bergslagen region, Sweden. Econ. Geol. 108, 309–335.
Johnson, I.R., Klingner, G.D., 1975. The Broken Hill ore deposit and its environment. In: Knight, C.L. (Ed.), Economic Geology of Australia and Papua New Guinea. Australasian Institute of Mining and Metallurgy Monograph 5, pp. 476–495.
Johnson, C.A., Rye, D.M., Skinner, B.J., 1990. Petrology and stable isotope geochemistry of the metamorphosed zinc–iron–manganese deposit at Sterling Hill, New Jersey. Econ. Geol. 85, 1133–1161.
Kaye, C.A., Mrose, M.E., 1965. Magnetic spherules, colored corundum, and other unusual constituents of a heavy beach sand, Martha's Vineyard, US. U.S. Geol. Surv. Prof. Pap. P0525-D, D37–D43.
Krauskopf, K.B., 1956. Factors controlling the concentrations of thirteen rare metals in sea-water. Geochim. Cosmochim. Acta 1, 1–32.
Krippner, A., Meinhold, G., Morton, A.C., von Eynatten, H., 2014. Evaluation of garnet discrimination diagrams using geochemical data of garnets derived from various host rocks. Sediment. Geol. 306, 36–52.
Larsen, R.B., Birkeland, A., Bjerkgård, T., 1997. Microcline gneisses in the Bleikvassli area: are they ore-genetic alteration zones or igneous intrusive rocks? Frank Vokes 70th Year Anniversary Symposium, Formation and Metamorphism of Massive Sulphides, Norwegian University of Science and Technology, Trondheim, Norway, p. 13
Leach, D.L., Sangster, D.F., Kelley, K.D., Large, R.R., Garven, G., Allen, C.R., Gutzmer, J., Walters, S., 2005. Sediment-hosted lead–zinc deposits: a global perspective. Society of Economic Geologists 100th Anniversary Volumepp. 561–607.
Lockington, J.A., Cook, N.J., Ciobanu, C.L., 2014. Trace and minor elements in sphalerite from metamorphosed sulphide deposits. Mineral. Petrol. 108, 873–890.
Longerich, H.P., Jackson, S.E., Günther, D., 1996. Laser ablation inductively coupled plasma mass spectrometric transient signal data acquisition and analyte concentration calculation. J. Anal. At. Spectrom. 11, 899–904.
McClenaghan, M.B., 2005. Indicator mineral methods in mineral exploration. Geochem. Explor. Environ. Anal. 5, 233–245.
McClenaghan, M.B., Kjarsgaard, B.A., 2001. Indicator mineral and geochemical methods for diamond exploration in glaciated terrain in Canada. In: McClenaghan, M.B., Bobrowsky, P.T., Hall, G.E.M., Cook, S.J. (Eds.), Drift Exploration in Glaciated Terrain. Geological Society (London), Special Publication 185, pp. 83–123.
McClenaghan, M.B., Hicken, A.K., Paulen, R.C., Layton-Matthews, D., 2012. Indicator mineral counts for regional till samples around the Izok Lake Zn–Cu–Pb–Ag VMS deposit, Nunavut. Geol. Surv. Can. Open File 7029 (13 pp.).
Metsger, R.W., 2001. Evolution of the Sterling Hill zinc deposit, Ogdensburg, Sussex County, New Jersey. Soc. Econ. Geol. Guideb. 35, 75–88.
Morris, T.F., Breaks, F.W., Averill, S.A., Crabtree, D.C., McDonald, A., 1997. Gahnite composition: implications for base metal and rare-element exploration. Explor. Min. Geol. 6, 253–260.
Murray, J.W., Spell, B., Paul, B., 1983. The contrasting geochemistry of manganese and chromium in the eastern tropical Pacific Ocean. In: Wong, C.S., Boyle, E.A., Bruland, K.W., Burton, J.D., Goldberg, E.D. (Eds.), Trace Metals in Seawater. NATO Conference Series: IV: Marine Science 9, pp. 43–669.
Nachtegaal, M., Marcus, M.A., Sonke, J.E., Vangronsveld, J., Livi, K.J.T., Van Der Lelie, D., Sparks, D.L., 2005. Effects of in situ remediation on the speciation and bioavailability of zinc in smelter contaminated soil. Geochim. Cosmochim. Acta 69, 4649–4664.
Nadoll, P., Mauk, J.L., Hayes, T.S., Koenig, A.E., Box, S.E., 2012. Geochemistry of magnetite from hydrothermal ore deposits and host rocks of the Mesoproterozoic Belt Supergroup, United States. Econ. Geol. 107, 1275–1292.
Nadoll, P., Angerer, T., Mauk, J.L., French, D., Walshe, J., 2014. The chemistry of hydrothermal magnetite: a review. Ore Geol. Rev. 61, 1–32.
Nehring, F., Foley, S.F., Hölttä, P., 2010. Trace element partitioning in the granulite facies. Contrib. Mineral. Petrol. 159, 493–519.
O'Brien, J.J., Spry, P.G., Teale, G.S., Jackson, S.E., Rogers, D., 2013. Trace element partitioning between gahnite, garnet, and biotite in gahnite-bearing rocks: implications for metamorphic processes and exploration for Pb–Zn–Ag mineralization. Society of Economic Geologists meeting (Whistler, British Columbia), pp. 45–46 (Abstract Volume).
O'Brien, J.J., Spry, P.G., Raat, H., Allen, R.S., Jansson, N., Frank, K.S., 2014. The major trace element chemistry of garnet in metamorphosed hydrothermal alteration zones, Stollberg Zn–Pb–Ag–(Cu–Au) ore field, Bergslagen district, Sweden: implications for exploration. Society of Economic Geologists SEG 2014 Conference, Keystone, Colorado, Abstract 0393-000185.
O'Brien, J.J., Spry, P.G., Nettleton, D., Xu, R., Teale, G.S., 2015a. Using Random Forests to distinguish gahnite compositions as an exploration guide to Broken Hill-type Pb–Zn–Ag deposits in the Broken Hill domain, Australia. J. Geochem. Explor. 146, 74–86.
O'Brien, J.J., Spry, P.G., Teale, G.S., Jackson, S., Rogers, D., 2015b. Major and trace element chemistry of gahnite as an exploration guide to Broken Hill-type Pb–Zn–Ag mineralization in the Broken Hill Domain, New South Wales, Australia. Econ. Geol. 110, 1027–1057.
Pagé, P., Barnes, S.-J., 2009. Using trace elements in chromites to constrain the origin of podiform chromitites in the Thetford mines ophiolite, Québec, Canada. Econ. Geol. 104, 997–1018.
Piercey, S.J., 2009. Lithogeochemistry of volcanic rocks associated with volcanogenic massive sulphide deposits and applications to exploration. In: Cousens, B., Piercey, S.J. (Eds.), Submarine Volcanism and Mineralization: Modern Through Ancient: Geological Association of Canada, Short Course Volume, 29–30 May 2008, Quebec City, Canada, pp. 15–40.
Raveggi, M., Giles, D., Foden, J., Raetz, M., 2007. High Fe–Ti mafic magmatism and tectonic setting of the Paleoproterozoic Broken Hill Block, NSW, Australia. Precambrian Res. 156, 55–84.
Raveggi, M., Giles, D., Foden, J., Raetz, M., Ehlers, K., 2008. Source and significance of the felsic magmatism in the Paleoproterozoic to Mesoproterozoic Broken Hill Block, New South Wales. Aust. J. Earth Sci. 55, 531–553.
Ridley, I.W., 2012. Petrology of associated igneous rocks in volcanogenic massive sulfide occurrence model. U.S. Geological Survey Scientific Investigations Report 2010-5070-C 15 (32 pp.).
Rocholl, A., 2008. Major and trace element composition and homogeneity of microbeam reference material. Basalt glass USGS BCR-2G. Geostand. Newslett. 22, 33–45.
Rosenberg, J.L., Spry, P.G., Jacobson, C.E., Cook, N.J., Vokes, F.M., 1998. Thermobarometry as applied to the Bleikvassli Zn–Pb–(Cu) deposit, Nordland, Norway. Mineral. Deposita 34, 19–34.
Ryan, P.J., Lawrence, A.L., Lipson, R.D., Moore, J.M., Paterson, A., Stedman, D.P., Van Zyl, D., 1986. The Aggeneys base metal sulphide deposits, Namaqualand district. In: Anheusser, C.R., Maske, S. (Eds.), Mineral deposits of Southern Africa: Geological Society of South Africa I and II, pp. 1447–1473.
Scott, K.M., Radford, N.W., 2007. Rutile compositions at the Big Bell Au deposit as a guide for exploration. Geochem. Explor. Environ. Anal. 7, 353–361.
Seifert, W., Rhede, D., Thomas, R., Förster, H.-J., Lucassen, F., Dulski, P., Wirth, R., 2011. Distinctive properties of rock-forming blue quartz: inferences from a multi-analytical study of submicron mineral inclusions. Mineral. Mag. 75, 2519–2534.
Sheridan, D.M., Raymond, W., 1984. Precambrian deposits of zinc–copper–lead sulfides and zinc spinel (gahnite) in Colorado. U.S. Geol. Surv. Bull. 1550 (31 pp.).
Shulters, J.C., Bohlen, S.R., 1989. The stability of hercynite and hercynite–gahnite spinels in corundum- or quartz-bearing assemblages. J. Petrol. 30, 1017–1031.
Simhachalam, J., Rao, M.S., 2004. Ore mineralogy of Mamandur polysulphide deposit, South Arcot District, Tamil Nadu. Spec. Publ. Ser. Geol. Surv. India 345–356.
Skauli, H., On the formation of Zn–Pb deposits: a case study of the Bleikvassli deposit, northern Norway. Unpublished Ph.D. thesis, University of Oslo, 1992, 194 pp.
Skauli, H., 1993. A metamorphosed, potassic alteration zone associated with the Bleikvassli Zn–Pb–Cu orebody, northern Norway. Lithos 31, 1–15.
Spry, P.G., 1978. The geochemistry of garnet-rich lithologies associated with the Broken Hill orebody. Unpublished M.S. thesis, University of Adelaide, N.S.W., Australia, p. 129.
Spry, P.G., 1987. The chemistry and origin of zincian spinel associated with the Aggeneys Cu–Pb–Zn–Ag deposits, Namaqualand, South Africa. Mineral. Deposita 22, 22–268.
Spry, P.G., Scott, S.D., 1986. The stability, synthesis, origin and exploration significance of zincian spinels. Econ. Geol. 81, 1446–1463.
Spry, P.G., Teale, G.S., 2009. Gahnite composition as a guide in the search for metamorphosed massive sulfide deposits. International Association of Applied Geochemists: Indicator Mineral Workshop B, Fredericton, New Brunswick, May 2009, pp. 27–34.
Spry, P.G., Heimann, A., Teale, G.S., 2004. Gahnite–garnet–staurolite relations to Proterozoic Broken Hill-type Pb–Zn–Ag mineralization in the Mutooroo area, Broken Hill Domain, South Australia. Geol. Soc. Am. Abstr. Programs 36, 19.
Spry, P.G., Teale, G.S., Steadman, J.A., 2009. Classification of Broken Hill-type Pb–Zn–Ag deposits: A refinement. Eos Transactions AGU 90, Joint Assembly Supplement, Abstract.
Spry, P.G., Both, R.A., Ogierman, J., McElhinney, R., Heimann, A., 2010. Origin of the Angas Pb–Zn–Ag deposit, Strathalbyn, South Australia. Society of Economic Geologists SEG 2010 Conference, Keystone, Colorado, Extended Abstracts, Abstract D-19 (3 pp.).
Spry, P.G., O'Brien, J.J., Frank, K.S., Teale, G.S., Koenig, A., Jansson, N., Allen, R., Raat, H., 2015. Trace element compositions of silicates and oxides as exploration guides to metamorphosed massive sulphide deposits: examples from Broken Hill, Australia, and Stollberg, Sweden. 27th International Association of Applied Geochemists: Indicator Mineral Workshop, Tucson, April 2015, 23–29.
Stanton, R.L., 1994. Ore Elements in Arc Lavas. Clarendon Press, Oxford (391 pp.).
Steadman, J.A., Spry, P.G., 2015. Metamorphosed Proterozoic Zn–Pb–Ag mineralization in the Foster River area, northern Saskatchewan, Canada. Econ. Geol. 110, 1193–1214.
Toteff, S., 1999. Cambrian sediment-hosted exhalative base metal mineralization, Kanmantoo Trough, South Australia. Geol. Surv. South Aust. Rep. Inv. 57 (41 pp.).

Trefry, J.H., Metz, S., 1989. Role of hydrothermal precipitates in the geochemical cycling of vanadium. Nature 342, 531–533.
Van Achterbergh, E., Ryan, C.G., Jackson, S.E., Griffin, W., 2001. Data reduction software for LA-ICP-MS. Mineral. Assoc. Can. Ser. 29, 239–243.
Volkert, R.A., Aleinikoff, J.N., Fanning, C.M., 2010. Tectonic, magmatic, and metamorphic history of the New Jersey Highlands: new insights from SHRIMP U–Pb geochronology. Geol. Soc. Am. Mem. 206, 307–346.
Walters, S.G., 1998. Broken Hill-type Pb–Zn–Ag deposits. AGSO J. Aust. Geol. Geophys. 17, 229–237.
Whitney, D.L., Evans, B.W., 2010. Abbreviations for names of rock-forming minerals. Am. Mineral. 95, 185–187.